Truss topology optimization of timber–steel structures for reduced embodied carbon design

Truss topology optimization of timber-steel structures for reduced embodied carbon design

Ernest Ching and Josephine V. Carstensen[1,*]

77 Massachusetts Ave., Cambridge, MA

Department of Civil and Environmental Engineering, Massachusetts Institute of Technology[1,*]

Abstract

There is an increasing need for automated design processes that can help guide structural design towards lower embodied carbon solutions. This research presents a two-material truss topology optimization algorithm that aims at reducing the Global Warming Potential (GWP) of the designed structure. The ground structure approach is used and a new set of design variables are defined such that both the cross-sectional area and the material composition of each truss element is determined. The framework is developed for several different objective and constraint functions. These include designing for a minimum compliance objective with either weight or GWP constraints, and minimizing the GWP with stress constraints. The framework is demonstrated on truss designs with a mix of glue-laminated timber (GLT) and steel elements on both 2D and 3D design examples.

Keywords: Topology Optimization, Timber-Steel, Truss, Embodied Carbon, Global Warming Potential

1. Introduction

The building and construction industry is a major source of carbon and greenhouse gas emissions, e.g. accounting for 39% of the annual global carbon emissions in 2017 [1]. Typically, the construction related emissions are categorized as either the operational carbon that is proportional to the energy used for building operations (e.g. lighting, heating/cooling, etc.), and the embodied carbon that relates to material extraction and preparation, transportion to sites, construction processes, maintenance, and demolition. Operational carbon

*Corresponding author

Email address: jvcar@mit.edu (Department of Civil and Environmental Engineering, Massachusetts Institute of Technology)

generally constitutes a larger fraction of building carbon footprints than the embodied carbon [2]. However, with the recent emphasis of lowering the operational energy requirements, the embodied carbon of buildings become increasingly important to consider [3, 4].

Several studies have proposed tools to measure and benchmark the embodied carbon content of buildings [5, 6, 7, 8]. To aid designers, Pomponi and Moncaster [9] highlight several mitigation strategies to lower the embodied carbon. Specifically, it is mentioned that significant savings can be obtained e.g. by using (i) more environmentally friendly materials, and (ii) structural optimization. However, at current there is a lack of design methods that aim at reducing the structural embodied carbon footprint [10].

The European Technical Committee TC350 [11] defines four stages of a building's life cycle in which contributions to the embodied carbon can occur. In a Life Cycle Assessment (LCA), carbon emissions associated with all stages of the life cycle should be included [12]. The structural elements most often accounts for the largest proportion of the entire embodied carbon [13]. Therefore, this work focuses on constraining or minimizing the embodied carbon associated with the product stage of the structural elements of new construction. This includes the carbon associated with the raw material supply, and transport to a factory for manufacturing of the structural components. A full LCA is not performed and transportation of construction materials and components to the specific construction site is not included in the current work. It should here be noted that this work relies on using site specific carbon inventory databases for construction materials and components. At current, some databases might not be able to provide carbon coefficients that cover all processes associated with the product stage. The relative difference in the used values will in some cases effect the design solutions. For some design scenarios, database values might only be available for location specific raw material use. In those cases, the herein presented framework will still allow designers to generate structural design solutions that are carbon efficient in terms of the raw material use. Further, it should be emphasized that the embodied carbon related to restoration or repurposing over the lifetime of the structure is not considered herein.

To estimate the embodied carbon of a whole structure or building, the Global Warming Potential (GWP) is convenient to use [14]. The GWP is defined as the sum of the material quantity of each material times the embodied carbon coefficient associated with the material:

$$GWP = \sum_{material}^{n} \sum_{i=1} (V_i \rho_i \times ECC_i), \tag{1}$$

where V_i and ρ_i are the volume and density of material i and ECC_i is the material's embodied carbon coefficient. If a structure consists of a single material, the GWP is directly proportional to the weight of the structure. In this case, structural optimization methods that minimize the weight will therefore also minimize the GWP. However, if a structure consists of multiple materials, it is not sufficient to solely minimize the structural weight.

More environmentally friendly materials tend to be combined with more common structural materials to make up for relative strengths and weaknesses that occur with changing of the loading directions. For example, timber and steel are often combined in trusses, as timber is 30% weaker in tension caused by non-uniformity in the wood grain orientations [15] while steel is more susceptible to compression buckling due to its slenderness. Moreover, timber is a more environmentally friendly material, with an ECC that is 3.5 times smaller than that of steel [16].

This paper focuses on truss design with reduced GWP as there is relatively little existing research on the topic. Brown and Mueller [17] used multi-objective optimization to find planar steel truss geometries for long span building roofs that optimize embodied and operational energy. Stern et al. [18] extended the planar roof trusses to multiple materials (timber and steel) and used shape and sizing optimization on various spans. It was found that compared to a baseline all-steel truss, a steel-timber truss can yield savings of 31% - 57% depending on the span length. This work seeks to go further by using truss topology optimization that increases the design freedom, and demonstrate the algorithm on both 2D and 3D timber-steel design examples.

Topology optimization is a freeform design approach where member sizes and connectivity are found through an iterative design process [19]. The design problem is formulated as a formal optimization problem and solved using a rigorous mathematical program. Although both objective and constraint functions can be chosen by the design engineer, most approaches typically consider a minimum compliance problem (equilvanlent to maximizing the stiffness for elastic, static conditions) that is subject to a weight constraint. While topology optimization has been used extensively in mechanical and aerospace applications

where it has been shown to lead to new solutions that typically outperform conventional low-weight design [19], its use in structural design is still relatively limited. The existing examples include using continuum and discrete element topology optimization for tall buildings [20, 21, 22, 23], design strut-and-tie layouts for reinforced concrete structures [24, 25, 26, 27, 28], and more recently to explore design of super-long spanning girder bridges [29].

Although, there exists several formulations for multi-material continuum topology optimization (e.g. [30, 31, 32]), most truss topology optimization focuses on single-material design. The main reserach emphasis has been on designing for minimum compliance or weight subject to stress and local buckling constraints [33, 34, 35, 36, 37]. Extensions have also addressed global buckling considerations [38, 39, 40]. The few works that consider multiple material properties include Achtziger [41] that used a single base material with different allowable stress limits in tension and compression. Stolpe and Svanberg [42] extended single material truss design to enable the selection between a finite number of predefined materials of each bar in minimum weight problems. This was done by introducing additional design variables. Stolpe and Svanberg [42] proved that at most two materials are sufficient in an optimal truss. Rakshit and Ananthasuresh [43] later allowed material selection of truss members from a database, with the goal of having the final design consist of a single material system.

This work will develop a new truss topology optimization framework for two-material design and demonstrate its applicability for several objectives and constraints. The two materials used for demonstration in the current work will be glue-laminated timber (GLT) and steel. The paper is organized as follows: for completness a brief introduction of single-material truss topology optimization with the ground structure approach is given in Section 2. This is followed by an extension to two-material design for stiffness objectives with either weight or GWP constraints in Section 3. Section 4 extends to designing with two materials for a a minimum GWP objective subject to stress constraints. Finally, Section 5 recasts the stress-constrained problem as a Mixed Integer Program and discusses possible future extensions.

2. Single-Material Truss Topology Optimization

This section gives a brief introduction to truss topology optimization using the ground structure approach [44] and a single material for all truss members. The ground structure approach is based on defining a dense ground structure with many potential elements and subsequently performing a generalized sizing optimization, where the minimum bar area is allowed to approach zero. The design engineer must define a design domain Ω with applied loads and boundary conditions. This domain is then densely populated with potential truss elements. In its most simple form, the problem is often formulated with the objective f of minimizing the compliance subject to a weight constraint g_w:

$$\begin{aligned} \underset{A^e}{\text{minimize}} \quad & f = \mathbf{F}^T\mathbf{d} \\ \text{subject to} \quad & \mathbf{K}(A^e)\mathbf{d} = \mathbf{F} \\ & g_w = \textstyle\sum_{e\in\Omega} A^e L^e \rho^e \leq W \\ & A_{min} \leq A^e \leq A_{max} \quad \forall\ e \in \Omega \end{aligned} \tag{2}$$

In Eq. (2) A^e denotes the cross-sectional area of element e, L^e is the member length and ρ^e is the material density of the member. The design variables are the cross-sectional areas A^e and these are bound by the user defined settings A_{min} and A_{max}. This work does not apply an explicit upper bound for the cross-sectional areas and uses $A_{min} = 10^{-3}$ for all examples. In addition to the weight constraint, the structure must also fulfill the static equilibrium condition. Here $\mathbf{F}$ is the global force vector, $\mathbf{d}$ is the global displacement vector, and $\mathbf{K}$ is the global stiffness matrix.

Figure 1 shows an example of a 2D cantilever beam problem with the defined design domain, the initial ground structure and the design obtained by solving Eq. (2). It is seen that through the optimization, some section sizes are reduced to (near) zero, while others increase in size such that a uniform stress distribution across all members is achieved. The design in Fig. 1c is, as all designs in this work unless otherwise stated, obtained in MATLAB 2020b using fmincon [45] as the gradient based optimizer.

All members with section areas below $A_{threshold} = 0.1$ have been removed from the plot in Fig. 1c. However, the solution still exhibits some of the undesired properties that may arise when using the ground structure approach. As an example, the solution contains

colinear elements connected by hinges that would result in an unstable structure if built as is. Even though all colinear elements should be merged in a post-processing step prior to construction, we have left them in the illustrations throughout this paper to ease reproducability of the results. A comprehensive list of the issues associates with the ground structure approach is provided by Ohsaki [46].

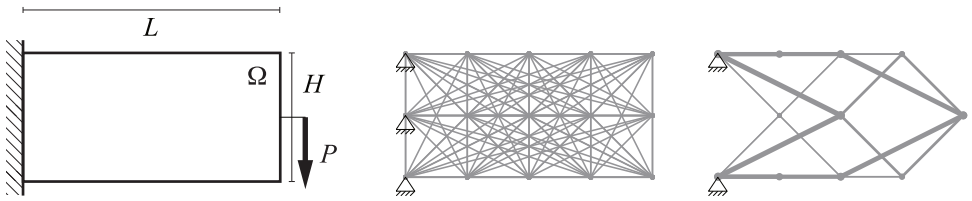

Figure 1: Cantilever beam 2D truss topology optimization problem with a single material for all members: (a) design domain where $L = 5.08$ m (200 in) and $H = 2.54$ m (100 in), (b) ground structure, and (c) topology-optimized solution.

2.1. Sensitivities

In order to solve the design problem in Eq. (2) with a gradient-based optimizer, the sensitivities of the objective and constraints must be evaluated. Using the adjoint method, the sensitivity of the compliance objective takes the well-known scaled strain energy form:

$$\frac{\partial f}{\partial A^e} = -\mathbf{d}^{\mathbf{T}} \frac{\partial \mathbf{K}}{\partial A^e} \mathbf{d} \tag{3}$$

We will here recall that for truss elements, the local element stiffness matrix is defined as follows:

$$\mathbf{k}^e = \frac{A^e E^e}{L^e} \begin{bmatrix} 1 & -1 \\ -1 & 1 \end{bmatrix}. \tag{4}$$

Following a standard FEA procedure, the local element stiffness matrix $\mathbf{k}^e$ is rotated to form the global element stiffness matrix $\mathbf{K}^e$ using the transformation element matrix $\mathbf{T}^e$:

$$\mathbf{K}^e = [\mathbf{T}^e]^{\mathbf{T}} \mathbf{k}^e \mathbf{T}^e. \tag{5}$$

As $\mathbf{T}^e$ is independent of the member stiffness and cross-sectional area, we will in this

work define $\mathbf{K_0}^e$ as the scaled element stiffness matrix in global coordinates:

$$\mathbf{K_0}^e = \frac{1}{A^e E^e}\mathbf{K}^e \tag{6}$$

The partial derivative of $\mathbf{K}$ with respect to the cross-sectional area A^e only receives a contribution from the local stiffness matrix $\mathbf{K}^e$. Using Eq.s (6-5), the sensitivity of the local element stiffness matrix can be found as

$$\frac{\partial \mathbf{K}^e}{\partial A^e} = E^e \mathbf{K_0}^e. \tag{7}$$

The sensitivity for the weight constraint is found by simple differentiation:

$$\frac{\partial g_w}{\partial A^e} = L^e \rho^e. \tag{8}$$

3. Two-Material Truss Topology Optimization for Minimum Compliance

In this work we extend the single material truss topology optimization problem from Section 2 by introducing a new set of continuous design variables x^e. For each element, x^e will determine the material composition. The design problem formulation will thus aim at determining both the material composition x^e and the cross-sectional area A^e of each element. The number of design variables is therefore doubled in comparison to the single-material design problem in Eq. (2). For the timber-steel trusses studied in this work, x^e will vary between zero and 1, where $x^e = 0$ means that the element is of timber and $x^e = 1$ refers to a steel element.

It is worth noting that although x^e is defined as continuous design variables in this work, a practical solution requires x^e to take (near) discrete values. Within the context of restricting the cross sections of each member to be chosen from a given list of catalogue sections, the topic of truss-based topology optimization with a mix of discrete and continuous design variables has received considerable attention. Stolpe [47] provides a comprehensive review of the published works in this area and depicts how the focus has shifted from solving using deterministic heuristic to metaheuristic optimization methods. Here deterministic heuristics refers to methods that typically are based on solving a sequence of continuous subproblems

combined with rounding techniques (e.g. gradient-based optimizers as used in this work), whereas metaheuristic methods are stochastic in nature such as e.g. genetic algorithms. To combat the typically high cost associated with solving by either of these methods; especially to obtain convergence for high-dimensional problems, some works have suggested to use Mixed Integer Linear Programming (MILP) (e.g. [48, 49]). Mela [50] suggests a MILP formulation for truss topology optimization with discrete sections that is able to capture the correct buckling length of compression members for both Euler and Eurocode specified buckling constraints. Van Mellaert et al. [51] formulates a truss sizing problem with discrete section areas and Eurocode specified displacement and joint constraints as a MILP. More recently, Fairclough and Gilbert [52] use MILP as the first stage in a two-step truss topology optimization design process, where the member sections are allowed to vary continuously and discrete variables are used to apply crossover joint constraint and thereby improve the constructability of the final design.

Although a Mixed Integer Program formulation could have been used for the herein targeted problem, this paper takes a different approach. Similar to the inclusion of stress constraints in a truss-based framework suggested by Bruggi [53], we herein draw inspiration from continuum topology optimization to include selection between two materials for all structural members.

For a minimum compliance objective, the following problem formulation is used:

$$
\begin{aligned}
\underset{A^e, x^e}{\text{minimize}} \quad & f = \mathbf{F}^T \mathbf{d} \\
\text{subject to} \quad & \mathbf{K}(A^e, x^e)\mathbf{d} = \mathbf{F} \\
& g \leq g_{max} \\
& A_{min} \leq A^e \leq A_{max} \quad \forall\ e \in \Omega \\
& 0 \leq x^e \leq 1 \quad \forall\ e \in \Omega.
\end{aligned}
\tag{9}
$$

Note that in Eq. (9), that the global stiffness matrix now depends both on the cross-sectional areas and the material compositions of the elements.

Eq. (9) is in this work solved with two different constraints g: (i) a weight constraint ($g = g_w$) as defined in Eq.(2), and (ii) a GWP constraint ($g = g_{GWP}$). The latter is defined

as:

$$g_{GWP} = \sum_{e \in \Omega} A^e L^e (\rho^e ECC^e) \leq GWP_{max}, \tag{10}$$

where ECC^e is the material embodied carbon coefficient and GWP_{max} is the user-specified global warming potential of the final structure.

It should here be noted that the application of an embodied carbon constraint does not in itself result in the design of environmentally friendly structures. If GWP_{max} is taken as an excessively high value compared to W, the opposite effect could in fact be achieved. The problem formulation for minimum compliance with $g = g_w$ in Eq. (2) is a widely used academic problem [19], even if a minimum weight with stiffness constraints is often preferable for practical applications. Some applications might benefit from being designed with a reasonable GWP constraint, especially when considering the life-cycle environmental impacts. It can be stipulated that GWP requirements might be specified in future design codes. A discussion on how to determine a reasonable GWP limit can be found in [54]. However, the current work is as previously stated, limited to considering the product stage of new construction. Since the environmental impacts associated with restoration and/or reuse is not included, direct minimization of the GWP is herein preferable. The alteration of the classical problem to include g_{GWP} instead of g_w should be seen as a step towards the formulation of a design problem that explicitly minimizes the embodied carbon.

3.1. Penalization of Intermediate Materials

Since continuous variables are needed for gradient based optimizers, we have introduced the material composition variables x^e as continuous variables. However, as previously mentioned, the desired outcome is a 0–1 design. Therefore, we make use the Solid Isotropic Material with Penalization (SIMP) [55] interpolation scheme. SIMP is traditionally used in continuum topology optimization to interpolate between void and solid elements. Here we will use SIMP to relate the material composition variables to the stiffness, density and global warming contributions of the elements:

$$E^e = (x^e)^\eta \Delta E + E_{timber}, \tag{11}$$

$$\rho^e = (x^e)^\eta \Delta \rho + \rho_{timber}, \tag{12}$$

$$(\rho^e ECC^e) = (x^e)^\eta \Delta(\rho ECC) + (\rho ECC)_{timber}. \tag{13}$$

In Eq.s (11-13), Δ refers to the difference between the steel and timber properties (e.g. $\Delta E = E_{steel} - E_{timber}$). The penalty exponent term η, makes the use of intermediate materials uneconomical and hence encourages the optimizer to converge to either $x^e = 0$ or $x^e = 1$. Unless otherwise stated, $\eta = 3$ is used within this work.

3.2. Sensitivities

For a compliance objective, the sensitivities with respect to the cross-sectional areas A^e remains as outlined in Section 2.1. The sensitivities with respect to the material composition variables x^e are derived in a similar manner. Using the adjoint method, it is found that:

$$\frac{\partial f}{\partial x^e} = -\mathbf{d^T}\frac{\partial \mathbf{K}}{\partial x^e}\mathbf{d}. \tag{14}$$

The partial derivatives of $\mathbf{K}$ with respect to x^e are found using the chain rule and differentiation of Eq. (11):

$$\frac{\partial \mathbf{K}}{\partial x^e} = \frac{\partial \mathbf{K}}{\partial E^e}\frac{\partial E^e}{\partial x^e} = A^e \mathbf{K_0}^e\big(\eta (x^e)^{\eta-1}\Delta E\big). \tag{15}$$

The sensitivity for the weight constraint case with respect to A^e is as in Eq. (8). Similarly, using differentiation of Eq. (12), the sensitivity with respect to the material composition variables is:

$$\frac{\partial g_w}{\partial x^e} = A^e L^e\big(\eta (x^e)^{\eta-1}\Delta \rho\big). \tag{16}$$

The sensitivities for the GWP constraint with respect to A^e and E^e are found as:

$$\frac{\partial g_{GWP}}{\partial A^e} = L^e(\rho^e ECC^e), \tag{17}$$

$$\frac{\partial g_{GWP}}{\partial x^e} = A^e L^e\big(\eta (x^e)^{\eta-1}\Delta(\rho\ ECC)\big). \tag{18}$$

3.3. Numerical Examples

The two-material topology optimization problems in Eq. (9) is solved with both weight (as in Eq. (2)) and embodied carbon (Eq. (10)) constraints for a range of 2D and 3D benchmark problems. The considered design domains with dimensions for all design problems are outlined in Fig. 1a and Fig. 2. The initial conditions were taken as $A_0^e = 6.5$ cm (1 in^2)

and $x_0^e = 0.5$ for all elements. The magnitude of the applied load is $P = 4.4$ N (1000 lb) for 2D problems and $P = 8.8$ N (2000 lb) for 3D problems. The weight constraint is prescribed as $W = 4.5 \cdot 10^5$ kg (10^6 lbs), and the GWP constraint as $GWP_{max} = 10^5$ $\text{kg}_{\text{CO}_2\text{e}}$ ($2.2 \cdot 10^5$ $\text{lbs}_{\text{CO}_2\text{e}}$).

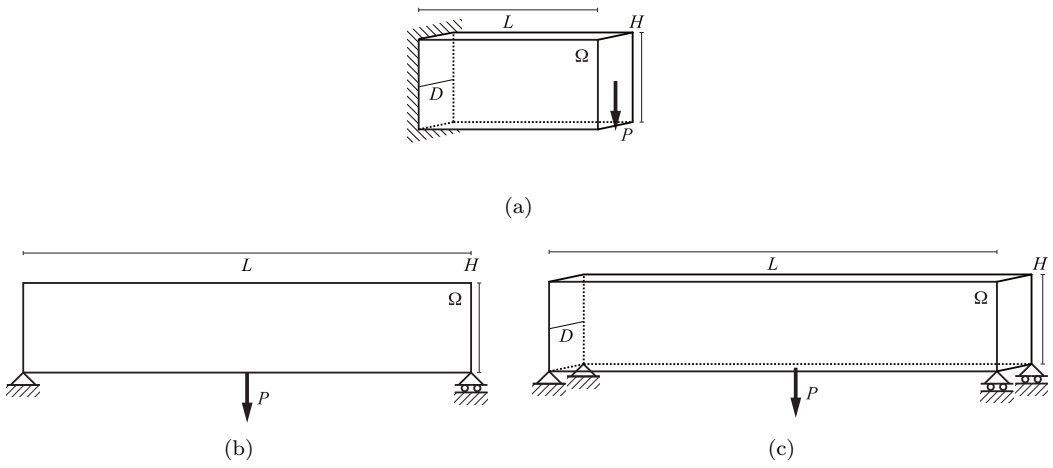

Figure 2: Design domains for tested benchmark problems; (a) a 3D cantilever with L and H as in Fig. 1, and $D = 2.54$ m (100 in), and (b) 2D and (c) 3D simply supported beams. For the simply supported beams $L = 12.7$ m (500 in), $H = 2.54$ m (100 in), and in (c) $D = 2.54$ m (100 in).

Since the ECC for a material will vary depending region, sourcing choice, building lifespan, and end-of-life treatment, the same material can be associated with an ECC of different magnitudes. To select an appropriate and consistent measure, this work uses ECC values from the Inventory of Carbon and Energy database [16]. Additionally, the material properties are taken for steel (50 ksi [56]) and Douglas Fir Grade L3 glue-laminated timber (GLT) [15]. All used property values herein are listed in Tab. 1.

Property		Steel	Timber	Property Ratio
E	(GPa)	200	11	18.2
σ_y	(MPa)	± 345	$-8.6/+6.6$	40.1/52.3
ρ	(kg/m^3)	7870	570	13.8
ECC	($\text{kg}_{\text{CO}_2\text{e}}/\text{kg}_{\text{material}}$)	1.45	0.42	3.5

Table 1: Properties taken for timber and steel in the current work and the ratio of each property taken as steel/timber (e.g. E_{steel}/E_{timber}).

Figure 3 gives the ground structures and solutions obtained by solving Eq. (9). Additionally, the final compliance value is listed for all examples. For all structures subjected to a weight constraint, the final solution is found to be an all-steel truss (Fig.s 3b,e,h,k). This

is not surprising since, as revealed by Tab. 1, steel is 18.2 times stiffer than timber, but only 13.8 times heavier. This means that steel is 1.3 times stiffer per unit weight than timber and explains why an all steel truss is preferable for stiffness objectives with weight constraints. In contrast, for design problems subjected to a GWP constraint, the final solutions consist
205 of all timber (Fig.s 3c,f,i,l). Timber can from Tab. 1 be deduced to be 2.6 times stiffer per unit mass of embodied carbon compared to steel and is therefore the preferred material in a maximum stiffness problem subject to a GWP constraint.

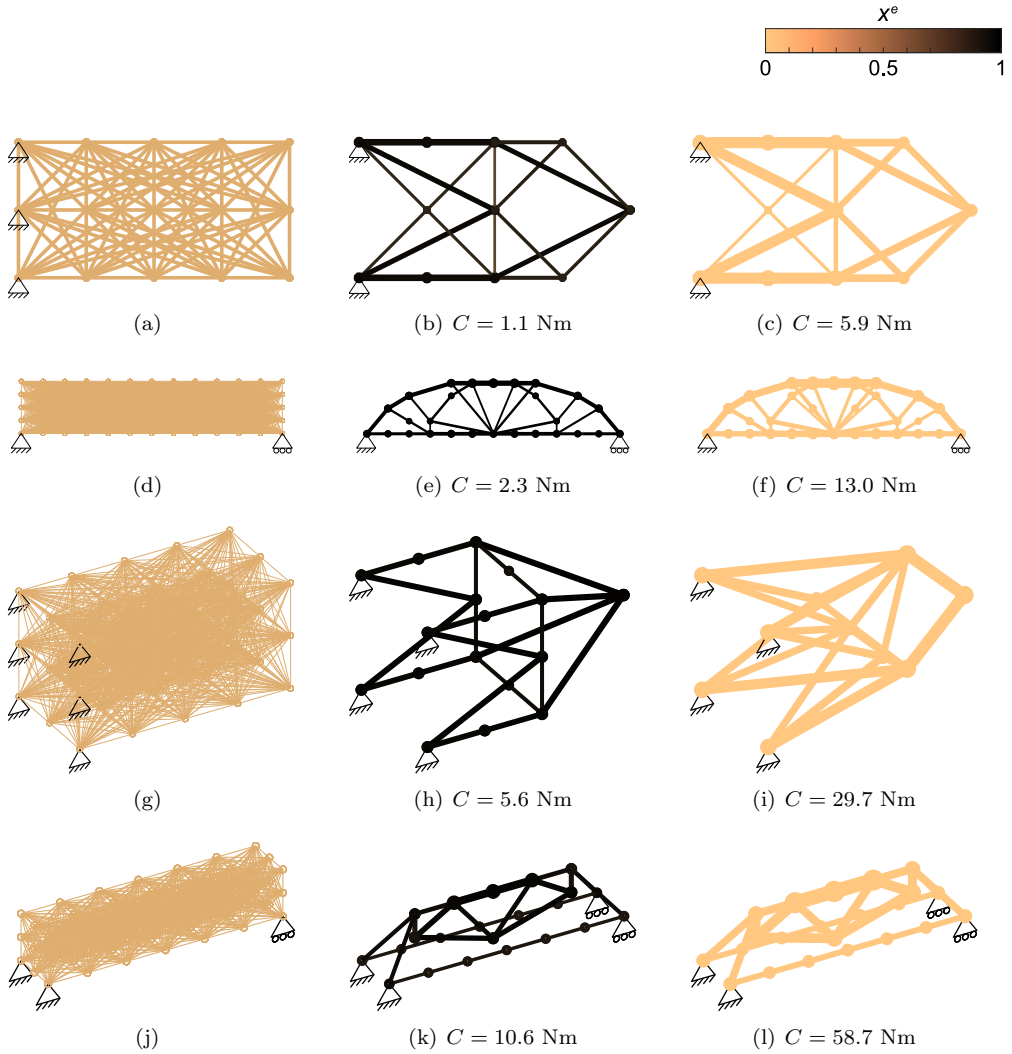

Figure 3: Designs obtained by solving Eq. (9). The ground structures are shown in (a), (d), (g), (j) and (b), (e), (h), (k) give the solutions obtained with $g = g_w$, whereas (c), (f), (i), (l) show the designs obtained with $g = g_{GWP}$.

The fact that the obtained solutions agree with the intuition on the most efficient mate-

rials to use for the considered design problems suggests that the extension to two-material design works as intended. It is worth noting, that for most examples very similar truss connectivities are obtained regardless of the constraint function (see Fig. 3), with section sizing differing. The suggested topology optimization framework is only convergent to a local minimum solution and obtaining the same connectivity was therefore not guaranteed as e.g. seen in Fig 3h-i. The trend of highly similar connectivities was, however, observed for most tested problems in this work.

4. Two-Material Trusses with Stress Constraints

Since the problem formulation in Eq. (9) only considers the material stiffness and does not consider the strength of each material, the optimizer is not encouraged to identify solutions that consists of multiple materials. In this work we have therefore formulated a design problem with the objective of minimizing the GWP subject to stress constraints. The following problem statement is used:

$$\begin{aligned} \underset{A^e, x^e}{\text{minimize}} \quad & \textstyle\sum_{e\in\Omega} A^e L^e (\rho^e ECC^e) \\ \text{subject to} \quad & \mathbf{K}(A^e, x^e)\mathbf{d} = \mathbf{F} \\ & \sigma^e_{min} \leq \sigma^e \leq \sigma^e_{max} \quad \forall\ e \in \Omega \\ & A_{min} \leq A^e \leq A_{max} \quad \forall\ e \in \Omega \\ & 0 \leq x^e \leq 1 \quad \forall\ e \in \Omega. \end{aligned} \tag{19}$$

The stress limits in Eq. (19) ensure that all elements in a resulting design will be stressed below the yield limit of the material and thus that the assumption of linear elastic behavior holds. For the timber-steel hybrid trusses considered in this work, the stress limits are defined as using a SIMP approach (similarly to the properties outlines in Eq.s (11-13)):

$$\sigma^e_{min} = (x^e)^{\eta_\sigma} \Delta\sigma_{min} + \sigma_{min,timber}, \tag{20}$$

$$\sigma^e_{max} = (x^e)^{\eta_\sigma} \Delta\sigma_{max} + \sigma_{max,timber}. \tag{21}$$

In addition to adding nonlinearity to the optimization problem, the application of stress constraints in truss optimization is known to give rise to a numerical issue, commonly

referred to as the stress singularity problem [57, 58, 59, 60, 61, 53]. The problem arises as the stress constraints should only be applied to members that actually appear in the design and not on members with areas that approach zero. Rozvany [60] gives an overview of the problem and lists methods for treating the numerical difficulties, including smooth envelope functions such as the ε-relaxation approach [59]. However, since this work uses a generalized sizing problem with a nonzero bound on the area that vanishes, the theoretical and computational issues with the design-dependent stress constraints disappear [47].

4.1. Sensitivities

The sensitivities for the stress constraints with respect to A^j and x^j are in this work derived using direct differentiation.

The sensitivities of the constraints $g_{\sigma,min}$ and $g_{\sigma,max}$ with respect to A^j are:

$$\frac{\partial g_{\sigma,min}}{\partial A^j} = -\frac{\partial \sigma^e}{\partial A^j}, \tag{22}$$

$$\frac{\partial g_{\sigma,max}}{\partial A^j} = \frac{\partial \sigma^e}{\partial A^j}. \tag{23}$$

To derive the partial derivate of σ^e with respect to A^j, recall the standard finite element computation procedure for truss elements:

$$\sigma^e = \frac{f^e}{A^e} = E^e \mathbf{T}^e \mathbf{K_0}^e \mathbf{d}^e, \tag{24}$$

where f^e is the axial force and $(1/A^e)\mathbf{K}^e$ as been substituted using Eq. (6). The derivative of Eq. (24) with respect to A^j is:

$$\frac{\partial \sigma_e}{\partial A^j} = E^e \mathbf{T}^e \mathbf{K_0}^e \frac{\partial \mathbf{d}^e}{\partial A^j}. \tag{25}$$

The term $\dfrac{\partial \mathbf{d}^e}{\partial A^j}$ is found as the element contribution of $\dfrac{\partial \mathbf{d}}{\partial A^j}$. By direct differentiation of the equilibrium constraint ($\mathbf{Kd} - \mathbf{F} = \mathbf{0}$), the derivative of $\mathbf{d}^e$ with respect to A^j can be extracted from:

$$\frac{\partial \mathbf{d}}{\partial A^j} = -\mathbf{K^{-1}} \left(\frac{\partial \mathbf{K}}{\partial A^j} \mathbf{d} \right) \tag{26}$$

Similarly, the sensitivities of the constraints $g_{\sigma,min}$ and $g_{\sigma,max}$ with respect to x^j are

derived by differentiating the stress constraints:

$$\frac{\partial g_{\sigma,min}}{\partial x^j} = \frac{\partial \sigma^e_{min}}{\partial x^e} - \frac{\partial \sigma^e}{\partial x^j}, \tag{27}$$

$$\frac{\partial g_{\sigma,max}}{\partial x^j} = \frac{\partial \sigma^e}{\partial x^j} - \frac{\partial \sigma^e_{max}}{\partial x^e}, \tag{28}$$

where $\frac{\partial \sigma^e_{min}}{\partial x^j}$ and $\frac{\partial \sigma^e_{min}}{\partial x^j}$ are found by differentiation of Eq.s (20-21) as:

$$\frac{\partial \sigma^e_{min}}{\partial x^j} = \begin{cases} \eta_\sigma (x^e)^{\eta_\sigma - 1} \Delta\sigma_{min} & \text{if } e = j \\ 0 & \text{otherwise,} \end{cases} \tag{29}$$

$$\frac{\partial \sigma^e_{max}}{\partial x^j} = \begin{cases} \eta_\sigma (x^e)^{\eta_\sigma - 1} \Delta\sigma_{max} & \text{if } e = j \\ 0 & \text{otherwise.} \end{cases} \tag{30}$$

The partial derivative of σ^e with respect to x^j in Eq.s (27-28) is found using the chain rule:

$$\frac{\partial \sigma^e}{\partial x^j} = \frac{\partial \sigma^e}{\partial E^j} \frac{\partial E^j}{\partial x^j}. \tag{31}$$

The partial derivate of E^j with respect to x^j take the same form as in Eq. (15). The derivative of the element stress σ^e with respect to E^j is found by differentiation of Eq. (24):

$$\frac{\partial \sigma^e}{\partial E^j} = \begin{cases} \mathbf{T}^e {\mathbf{K_0}}^e \mathbf{d}^e + E^e \mathbf{T}^e {\mathbf{K_0}}^e \dfrac{\partial \mathbf{d}^e}{\partial E^j} & \text{if } e = j, \\ E^e \mathbf{T}^e {\mathbf{K_0}}^e \dfrac{\partial \mathbf{d}^e}{\partial E^j} & \text{otherwise.} \end{cases} \tag{32}$$

where $\frac{\partial \mathbf{d}^e}{\partial E^j}$ is obtained similarly to $\frac{\partial \mathbf{d}^e}{\partial A^j}$ as the element contribution from:

$$\frac{\partial \mathbf{d}}{\partial E^j} = -\mathbf{K^{-1}} \left(\frac{\partial \mathbf{K}}{\partial E^j} \mathbf{d} \right) \tag{33}$$

4.2. Numerical Examples with Realistic Stress Limits

The stress constrained problem in Eq. (19) is initially solved using the material stress limits for timber and steel listed in Tab. 1. The SIMP interpolation for E^e and ECC^e is set to $\eta = 1$ and the intermediate stress constraints are penalized with $\eta_\sigma = 3$ to guide the optimizer towards 0–1 solutions for all x^e. The initial conditions are taken as $A_0 = 32.3$ cm^2 (5 in^2) and $x_0 = 0.5$, with a lower bound on A^e prescribed as $A_{min} = 6.5 \cdot 10^{-3}$ cm^2

$(10^{-3}$ in$^2)$.

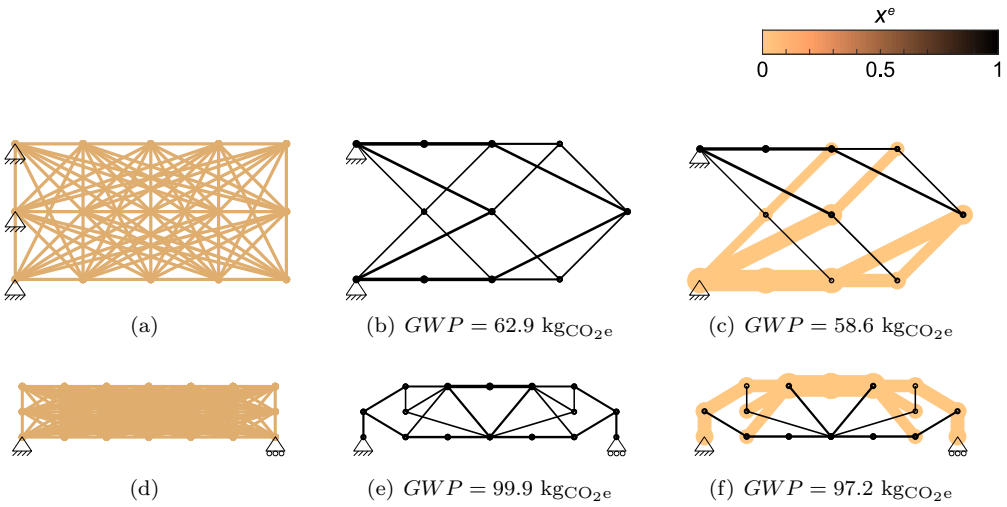

Figure 4: Designs obtained by solving Eq. (19) with realistic material stress limits as outlined in Tab. 2. Ground structures are shown in (a) and (d), and the design results for the 2D cantilever and simply supported beams are given in (b) and (e), respectively. Designs obtained by manually modifying the compressive members from (b) and (e) to timber are shown in (c) and (f).

Figure 4 shows the optimized designs obtained by solving Eq. (19) on the 2D cantilever and simply supported beam problems. The ground structures are shown in Fig. 4a,d and the optimized solutions are given in Fig. 4b,e. It is seen that using the realistic stress limits from Tab. 1 results in all steel trusses for both cases. This was generally observed for most tested problems. However, the all steel solutions are upon investigation found to be poor performing local minima. If manually changing all compression elements in the obtained trusses to timber elements (Fig. 4c,f), it is observed that the all steel solutions have a slightly higher GWP (6.8% and 2.6%, for the cantilever and simply supported beam, respectively).

4.3. Effect of Stress Limits on a Single Bar

To investigate why the optimizer tends to identify single-material solutions when realistic stress limits are applied, a simplified truss topology optimization problem of a single bar subject to an axial load is studied. The bar will in this work be subjected to two sets of stress limits; (i) the more realistic stress limits imposed in Section 4.2, and (ii) stress limits that are modified to force compressive members to be of timber, and tensile members to be of steel. These sets of limits are listed in Tab. 2.

	Limit		Steel	Timber
Realistic	σ_{min}	(MPa)	-345	-8.6
	σ_{max}	(MPa)	345	6.6
Modified	σ_{min}	(MPa)	0	-8.6
	σ_{max}	(MPa)	345	0

Table 2: Realistic and modified stress limits applied on single bar problems.

Figure 5 shows the single-bar ground structures and obtained topologies for both considered sets of stress limits. The load magnitude is for this example set to $P = 66.7$ kN (15 kips) and the length of the member is 38.1 cm (15 in). The initial conditions are chosen as $A_0 = 32.3$ cm^2 (5 in^2) and $x_0 = 0.5$.

Under the realistic stress constraints, the tensile bar converges to a steel bar (Fig. 5b). This was expected since steel is stronger in tension per unit embodied carbon. However, the compressed bar also converges to a steel bar in Fig. 5e, which is counterintuitive since timber is stronger in compression per unit embodied carbon. When employing the modified stress constraints that force compressive members to be of timber, the optimizer is guided to choose timber for a compressed bar (Fig. 5f). The global warming potential for the timber bar in compression is $GWP = 1.56$ kg$_{\mathrm{CO_2e}}$, which is lower than that of the steel bar in compression ($GWP = 1.87$ kg$_{\mathrm{CO_2e}}$).

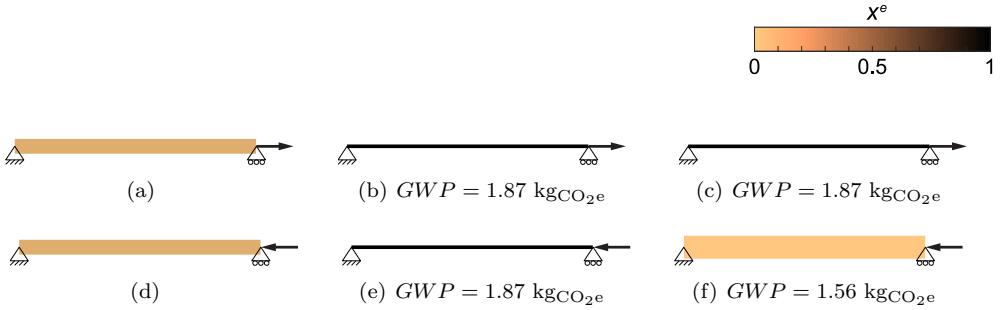

Figure 5: Single bar examples in (a–c) tension and (d–f) compression. The ground structures are given in (a) and (d), the obtained results with realistic stress limits are given in (b), (e) and the designs obtained with modified stress limits are shown in (c) and (f).

To illustrate why a better objective is obtained when using the modified stress constraints, graphical optimization is used to plot the feasible region for the single bar problems. When using graphical optimization here, the contours of the objective function is plotted on a graph that contains the design variable x on the x-axis and A on the y-axis.

The relevant constraint function is additionally added to the plot (here σ_{max} for the tension bar and σ_{min} for the compression bar). This allows the feasible region and the trends of the objective function to be clearly illustrated. The reader is referred to [62] for a detailed discussion on the steps associated with graphical optimization.

Figure 6 shows the graphical optimization plots for the two single bar examples. In Fig. 6a, for a single bar in tension, the problem correctly converges to the global minimum (steel) under the realistic stress constraints. In Fig. 6b, modifying the stress constraints (such that timber takes no load in tension) removes the local minimum at $x = 0$ (timber), which does not affect the direction of convergence, since the optimizer was already choosing the optimal material (steel) correctly.

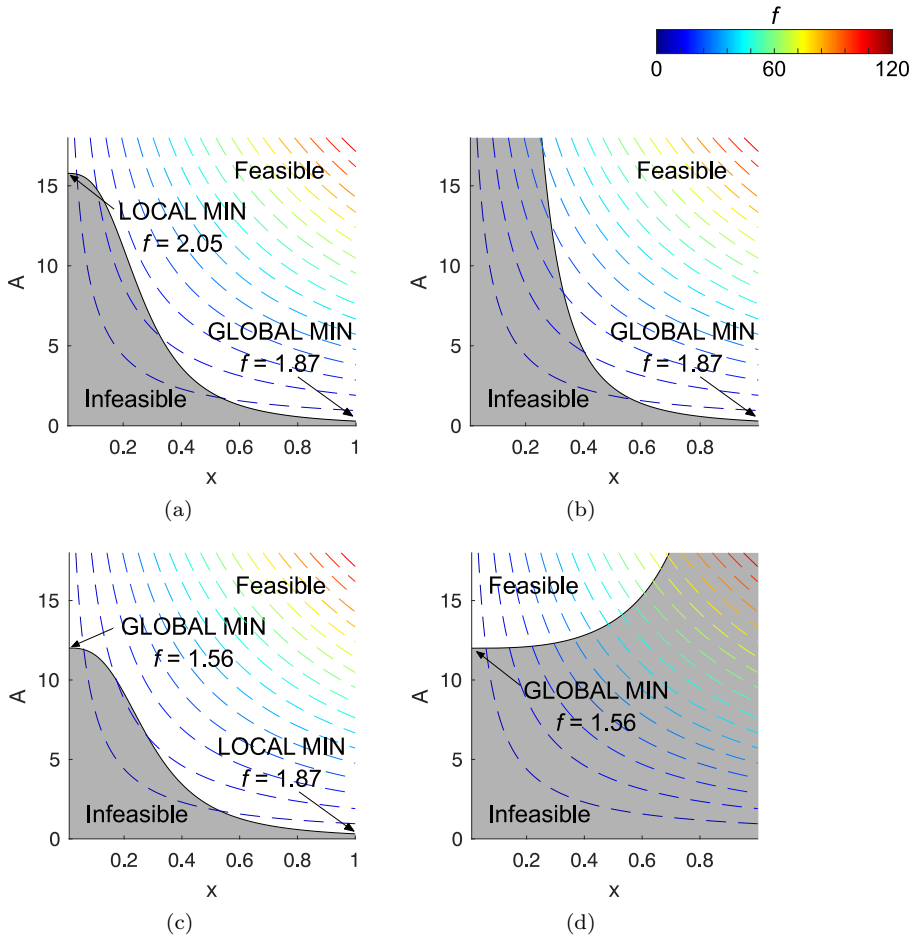

Figure 6: Graphical optimization of single bar problems in (a–b) tension and (c–d) compression. In (a) and (c) realistic stress limits are applied, whereas modified stress limits are specified in (b) and (d). The blue arrows indicate the direction of convergence.

In Fig. 6c, for a single bar in compression, the problem converges to a local minimum (steel) under realistic stress constraints, instead of the global minimum (timber). Studying the objective landscape, we can conclude that this is due to nonlinearities. As shown in Fig. 6c, the problem of being guided to a poor performing local minimum is for this case resolved by eliminating the local minimum itself. Modifying the stress constraints such that steel takes no load in compression removes the local minimum at $x = 1$ (steel), encouraging the optimizer to converge to the only minimum remaining, at $x = 0$ (timber).

It is recognized that modifying the stress limits as suggested herein reduces the design space significantly and removes design freedom from the user. However, in addition to eliminating nonlinearity from the optimization problem as shown, there are some practical advantages for the specific case of timber-steel trusses. Due to their typically high slenderness, compressive steel truss members are often governed by buckling failure. Although buckling considerations are not included in the current work and still may be important for some compressive timber bars, eliminating compressive steel reduces the limitations of the presented framework. Moreover, timber joints loaded in tension generally require carefull design to avoid catastrophic failure [63, 64]. These joints are herein eliminated by using the modified stress limits.

4.4. Numerical Examples with Modified Stress Limits

The stress constrained problem in Eq. (19) is re-solved using the modified stress limits from Tab. 2. All other parameters are taken as in Section 4.2.

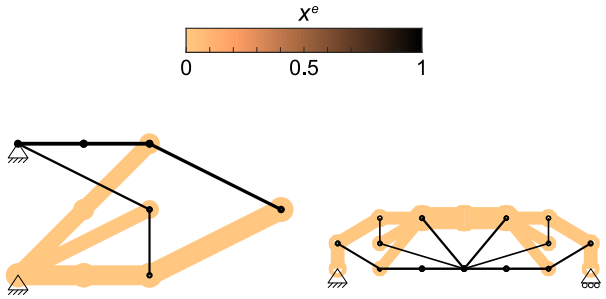

(a) $GWP = 57.5$ $\mathrm{kg_{CO_2e}}$ (b) $GWP = 90.2$ $\mathrm{kg_{CO_2e}}$

Figure 7: Designs obtained with modified stress limits for the 2D (a) cantilever and (b) simply supported beam problems. The ground structures from Fig. 4 are used.

Figure 7 shows the optimized designs obtained by solving Eq. (19) on the 2D cantilever

and simply supported beam problems. As expected, the solutions are seen to employ both steel and timber, with steel carrying tensile loads and timber resisting compressive loads. It is worth noting that the obtained topology for the cantilever design differs significantly from a single change of material in the compressive members of the solutions in Fig. 4 obtained with realistic stress limits. When comparing the GWP of the solutions in Fig. 4 and Fig. 7, it is seen that for both examples, the modified stress limits yield better performing designs. For the cantilever, the design obtained with realistic stress limits (Fig. 4b) is 9.4% more polluting than the modified stress solution (Fig. 7a). Similarly, the realistic stress solutions for the simply supported beam (Fig. 4d) is 10.8% more polluting than its modified stress counterpart (Fig. 7b).

The modified stress constraints are also tested on 3D cantilever and MBB beam problems and the solutions are shown in Fig. 8. As expected, the obtained structures resemble their 2D counterparts (Fig. 7) and consists of both timber and steel elements.

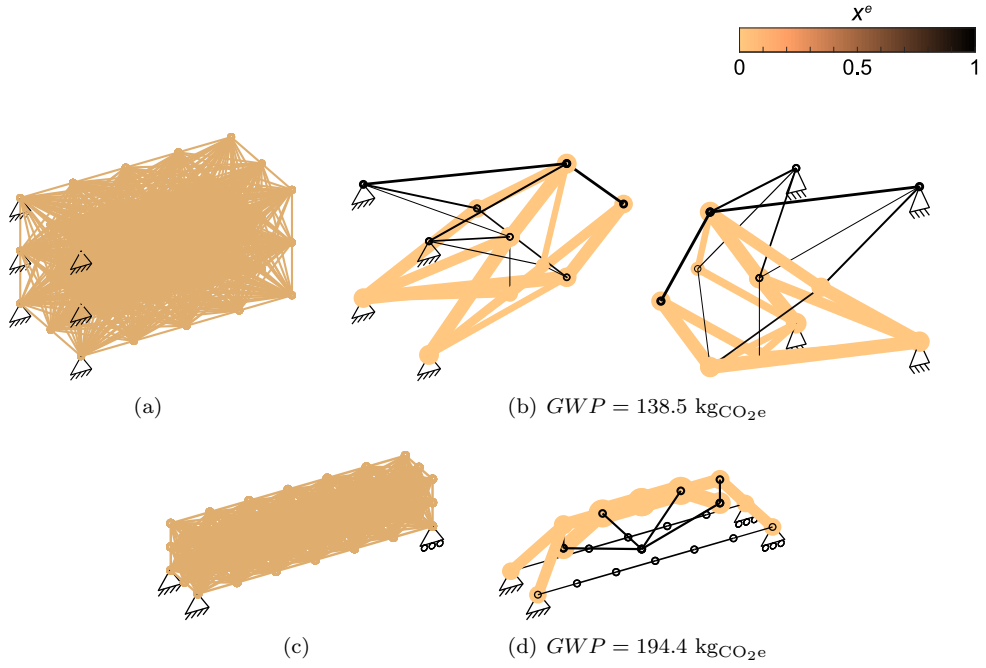

Figure 8: Ground structures and obtained designs with modified stress limits for the 3D (a-b) cantilever and (c-d) simply supported beam problems.

5. Two-Material Trusses with Stress Constraints as a Mixed Integer Quadratic Program

Despite this preliminary success, it is speculated that the increase of nonlinearity introduced through the presented framework may make it more difficult for the optimizer to identify quality solutions. This could especially pose problems if additional constraints must be considered e.g. local or global buckling or displacement constraints. Solving potential extensions of this work that include additional relevant design requirements such as multiple load cases and code constraints will likely benefit from being formulated using different solution methods such a Mixed Integer Program.

Since the GWP for a single material structure is directly proportional to the structural weight, single material truss topology optimization that minimizes the GWP with stress constraints can be formulated as the following linear program (for details on the classical minimum weight linear problem, the reader is e.g. referred to [65]):

$$\begin{aligned} \underset{\mathbf{A},\mathbf{q}}{\text{minimize}} \quad & f = (\rho ECC)\mathbf{L}^{\mathbf{T}}\mathbf{A} \\ \text{subject to} \quad & \mathbf{Bq} = \mathbf{F} \\ & -\sigma_{min}\mathbf{A} - \mathbf{q} \leq 0 \\ & -\sigma_{max}\mathbf{A} + \mathbf{q} \leq 0 \\ & \mathbf{A} \geq 0. \end{aligned} \tag{34}$$

Here the design variables are the vectors $\mathbf{A}$ and $\mathbf{q}$, where $\mathbf{A}$ contains the cross sectional areas and $\mathbf{q}$ the internal forces of all members in the ground structure. The static equilibrium is evaluated using $\mathbf{Bq} = \mathbf{F}$ where $\mathbf{B}$ is the strain displacement matrix.

The linear problem in Eq. (34) can, as previously, be extended to two materials by introducing the discrete material choice variables $x^e \in \{0, 1\}$. The material choice is now defined via a binary variable where $x^e = 0$ denotes a timber member, while $x^e = 1$ designates steel. When designing with two materials (here timber and steel), the contribution to the GWP from element e can as before be computed by:

$$GWP^e(A^e, x^e) = (\rho\ ECC)_{timber} A^e L^e + \Delta(\rho\ ECC) L^e A^e x^e, \tag{35}$$

where $\Delta(\rho\ ECC) = (\rho\ ECC)_{steel} - (\rho\ ECC)_{timber}$.

When discussing the extension to two materials in the context of a Mixed Integer Program, it is convenient to define a design variable vector $\mathbf{v}$ that contains the cross sectional area, internal member force and material choice vectors such that $\mathbf{v} = \{\mathbf{A}; \mathbf{q}, \mathbf{x}\}$. The GWP objective can be formulated as a quadratic function in $\mathbf{v}$:

$$GWP(\mathbf{v}) = (\rho ECC)_{timber}\mathbf{r^T v} + \Delta(\rho ECC)\mathbf{v^T Q v}, \tag{36}$$

In Eq. (36) $\mathbf{r} = \{\mathbf{L}; \mathbf{0}; \mathbf{0}\}$ and $\mathbf{Q}$ is largely a zero matrix, containing $1/2L^e$ on the off diagonal places corresponding to A^e and x^e multiplications. Let N be the number of bars in the ground structure and $e = \min\{i, j\}$:

$$Q_{i,j} = \begin{cases} 1/2A^eL^e & \text{if } j = i \pm 2N\ ,\ 0 \leq i, j \leq 3N \\ 0 & \text{otherwise.} \end{cases} \tag{37}$$

Using the objective in Eq. (36), the two material design problem that minimizes the GWP with stress constraints can be formulated as the following a Mixed Integer Quadratic Program (MIQP):

$$\begin{aligned} \underset{\mathbf{v}=\{\mathbf{A},\mathbf{q},\mathbf{x}\}}{\text{minimize}} \quad & f = (\rho ECC)_{timber}\mathbf{r^T v} + \Delta(\rho ECC)\mathbf{v^T Q v} \\ \text{subject to} \quad & \mathbf{Bq} = \mathbf{F} \\ & \sigma_{min,timber}\mathbf{A} - \mathbf{q} - q_{min}\mathbf{x} \leq 0 \\ & \sigma_{max,timber}\mathbf{A} - \mathbf{q} + q_{max}\mathbf{x} \geq 0 \\ & \sigma_{min,steel}\mathbf{A} - \mathbf{q} + q_{min}\mathbf{x} \leq q_{min} \\ & \sigma_{max,steel}\mathbf{A} - \mathbf{q} - q_{max}\mathbf{x} \geq q_{max} \\ & 0 \leq A^e \leq A_{max} \quad \forall\ e \in \Omega \\ & x^e \in \{0, 1\} \quad \forall\ e \in \Omega. \end{aligned} \tag{38}$$

Although it has no practical application for the resulting designs, it is worth nothing that the problem in Eq. (38) is not identical to the previously presented design problems in this work. In addition to discreteness of x^e being strictly enforced, there is a (potential) modeling discrepancy since the equilibrium condition is expressed differently.

In Eq. (38) the terms involving q_{min} and q_{max} are added to the stress constraints to

ensure that the material choice affects the stress limits. The values are in this work chosen as:

$$q_{min} = -\min\{\sigma_{min,timber}, \sigma_{min,steel}\} A_{max} \tag{39}$$

$$q_{max} = \max\{\sigma_{max,timber}, \sigma_{max,steel}\} A_{max} \tag{40}$$

The MIQP in Eq. (38) is in this work solved using the cutting plane method [66] as a series of MILP problems that satisfy the constraints, and that increasingly approximate the quadratic objective function. Eq. (38) is therefore reformulated to a problem with a linear objective and nonlinear constraints by introducing the slack variable $z \geq 0$ that represents the quadratic term through the inequality constraint $\mathbf{v^T Q v} - z \leq 0$. The objective thus becomes:

$$f = (\rho_{timber} ECC_{timber})\ \mathbf{r^T v} + (\Delta\rho\ ECC)\ z. \tag{41}$$

It can be shown that the for each intermediate solution $\mathbf{v}_k$, a new linear constraint approximates the nonlinear constraint locally using the following expression:

$$\mathbf{v}_k^\mathbf{T} \mathbf{Q} \mathbf{v}_k + 2\mathbf{v}_k^\mathbf{T} \mathbf{Q} \mathbf{v} - z \leq 0 \tag{42}$$

The Matlab function intlinprog is used to solve the MILPs. For ever MILP solved, a new constraint is added to the problem using Eq. (42) until z is sufficiently close to the true quadratic term.

Figure 9 gives an example design problem solved using both the herein suggested SIMP-based and MIQP approaches. The design problem is shown in Fig. 9a and herein solved using $L = 25.4$ cm (10 in), $H = 50.8$ cm (20 in), and $P = 4.45$ kN (10 kips). The used ground structure is shown in Fig. 9b and the upper bound on A^e is set to $A_{max} = 99.8$ cm^2 (15 in^2). The SIMP-based solution is obtained by solving Eq. (19) with the same parameter settings as previously. The MIQP solves Eq. (38) and solutions are in both cases obtained using both the realistic and modified stress limits from Tab. 2.

Figure 9c-d gives the design solutions obtained by solving the MIQP in Eq. (38). The designs obtained with the SIMP-based approach are given in Fig. 9e-f. It is clearly seen that the MIQP formulation encounters the same problems with nonlinearity as the SIMP-based

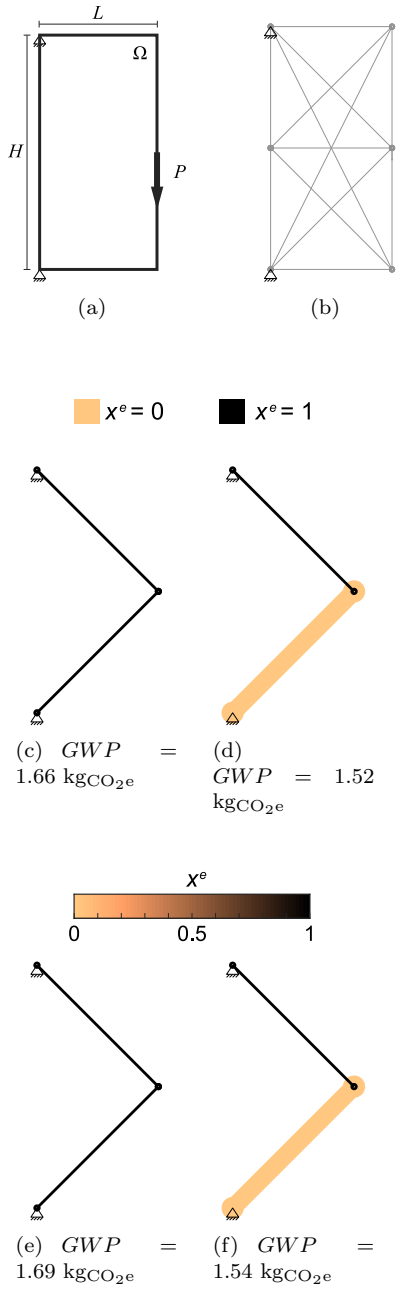

Figure 9: Illustration of (a) design domain, and (b) ground structure. Design solutions to the MIQP in Eq. (38) obtained with (c) realistic stress limits, and (d) modified stress limits. Solutions to the SIMP-based problem in Eq. (19) obtained with (e) realistic stress limits, and (f) modified stress limits.

360 approach. With both approaches, using realistic stress limits results in all steel solutions. Modification of the stress limits are for both approaches needed to obtain hybrid solutions that for the current example outperform the all steel design. The same trends are observed

for other tested cases.

Small improvements in the obtained GWP-values are observed when solving with the MIQP rather than the SIMP-based approach (e.g. Fig. 9c vs. Fig. 9e). This is due to the explicit integer constraint on x^e, which is only implicitly guided to 0–1 in the SIMP-based solution and thus exhibits small deviations.

Although recasting the design formulation using a MIQP does not solve the problem of nonlinearity, it does offer some advantages. Less post-processing of solutions is required as the minimum cross-sectional areas are allowed to take zero, eliminating the need to define a threshold and remove members with small sections. Moreover, adding additional linear constraints, such as e.g. Euler buckling, can easily and efficiently be done. However, the nonlinearity associated with the herein presented MIQP is found to be significant and obtaining quality solutions, especially for large ground structures, requires both algorithmic tuning and considerable computational power. For the problems considered herein, similarly or better performing solutions have been identified using the SIMP-based approach for all tested cases.

However, the potential associated with posing the design problem using mixed integer programming should not be underestimated. Identifying a way to formulate the GWP objective as a linear function (as opposed to a quadratic as in this work), would allow the design formulation to be cast directly as a MILP. This would solve to both the problems associated with nonlinearity and required computational resources. Such a formulation would likely be necessary to successfully solve potential extensions of this work that include additional relevant design requirements such as multiple load cases and code constraints.

6. Conclusion

A technique is proposed for topology optimization of truss structures with two materials for a range of objectives and constraints, including the embodied carbon. The embodied carbon is herein accounted for through the GWP of the first stage of the structures life cycle. The proposed framework allows the designer to automatically generate topology-optimized truss designs that incorporate elements of two distinct material systems, herein demonstrated for timber and steel. The design framework identifies both the material composition and the cross-sectional area of all members in the truss. A ground structure

approach is used where an additional set of design variables are introduce to account for the choice of material. The proposed approach relies on the design engineer having access to common material properties for both used materials, and when designing for the GWP the materials' embodied carbon coefficients must additionally be known.

Designs are presented for a minimum compliance objective, subject to both weight and GWP constraints. In line with intuition on best material choice for these problems, the resulting structures are found to contain only a single material; steel for weight constraints and timber for GWP constraints. The obtained single material designs thus demonstrates that the presented framework works as intended. In addition, the formulation is extended to minimize the GWP subject to stress constraints. Here it is found that the proposed formulation introduces a significant level of nonlinearity to the optimization problem, that circumvents using the realistic material stress limits for the design. Instead, it is found that modifying the stress limits such that timber only has the capability to carry compressive loads whereas steel only can carry tensile forces tends to yield better performing results. Across all studied structures, improvement by changing the stress limits was found to be 9.4%–10.8%. The design problem is recast as an MIQP, and here it is also seen that the modified stress limits provides better performing design solutions.

In the review paper by Stolpe [47], the need for proposing new application relevant combinations of objective and constraint functions is articulated in the hope that it will to spur the development of new theory, methods, and heuristics in the area of truss topology optimization. In addition to providing design engineers with tools for solving the specific design problems outlined herein, this work contributes to that end. Solving potential extensions of this work will likely required that the GWP can be formulated as a linear function, which is a topic worthy of future research.

A limitation of herein suggested approach is that it only considers the embodied carbon contributions associated with the first stage of the building's life cycle. Since life-cycle management criteria can be conflicting (e.g. minimizing the life-cycle cost and maximizing the expected service life) [67], an interesting future extension of this work could be the inclusion of a full LCA in the design problem formulation. For a site-specific design, a straightforward extension could be to include transportation of structural components to the site by multiplying the material specific embodied carbon coefficients with location specific

transportation costs. In a case where e.g. timber transportation is much longer than transportation from a steel component factory, multiplication with transportation costs will likely alter the design solutions. Additionally, studies have shown that designing for deconstruction and recycling have significant environmental benefits [68, 54]. An interesting avenue would therefore be the incorporating end-of-life design considerations as e.g. suggested by [69] for continuum topology-optimized designs.

References

[1] T. Abergel, B. Dean, J. Dulac, United Nations Environment Programme 48 (2017).

[2] C. R. Iddon, S. K. Firth, Energy and Buildings 67 (2013) 479–488.

[3] I. Sartori, A. G. Hestnes, Energy and buildings 39 (2007) 249–257.

[4] R. Giordano, V. Serra, E. Tortalla, V. Valentini, C. Aghemo, Energy Procedia 78 (2015) 3204–3209.

[5] R. J. Cole, P. C. Kernan, Building and environment 31 (1996) 307–317.

[6] A. Fudholi, K. Sopian, M. Y. Othman, M. H. Ruslan, Energy and Buildings 68 (2014) 121–129.

[7] C. De Wolf, F. Pomponi, A. Moncaster, Energy and Buildings 140 (2017) 68–80.

[8] P. Chastas, T. Theodosiou, K. J. Kontoleon, D. Bikas, Building and Environment 130 (2018) 212–226.

[9] F. Pomponi, A. Moncaster, Journal of environmental management 181 (2016) 687–700.

[10] T. Häkkinen, M. Kuittinen, A. Ruuska, N. Jung, Journal of Building Engineering 4 (2015) 1–13.

[11] B. BSI, et al. (2011).

[12] A. Moncaster, F. Pomponi, K. Symons, P. Guthrie, Energy and Buildings 173 (2018) 389–398.

[13] Z. Luo, L. Yang, J. Liu, Building and Environment 95 (2016) 365–371.

[14] C. De Wolf, F. Yang, D. Cox, A. Charlson, A. S. Hattan, J. Ochsendorf, in: Proceedings of the Institution of Civil Engineers-Engineering Sustainability, Thomas Telford Ltd, pp. 1–12.

[15] A. W. Council, American Wood Council (????).

[16] G. Hammond, C. Jones, F. Lowrie, P. Tse, Embodied carbon: the inventory of carbon and energy (ICE). Bracknell: BSRIA (????).

[17] N. C. Brown, C. T. Mueller, Energy and Buildings 127 (2016) 748–761.

[18] B. Stern, C. De Wolf, C. Mueller, in: C. Mueller, S. Adriaenssens (Eds.), Proceedings of IASS Annual Symposia, International Association for Shell and Spatial Structures (IASS), pp. 1–8.

[19] M. P. Bendsøe, O. Sigmund, Topology optimization: Theory, Methods and Applications, 1 ed., Springer-Verlag, Berlin, Germany, 2003.

[20] L. L. Stromberg, A. Beghini, W. F. Baker, G. H. Paulino, Structural and Multidisciplinary Optimization 43 (2011) 165–180.

[21] L. L. Stromberg, A. Beghini, W. F. Baker, G. H. Paulino, Engineering Structures 37 (2012) 106–124.

[22] S. Bobby, S. M. Spence, E. Bernardini, A. Kareem, Engineering Structures 74 (2014) 242–255.

[23] M. Zhu, Y. Yang, J. K. Guest, M. D. Shields, Structural Safety 67 (2017) 116–131.

[24] P. Kumar, Computers & Structures 8 (1978) 223–229. doi:10.1016/0045-7949(78)90026-3.

[25] Q. Q. Liang, Y. M. Xie, G. P. Steven, Structural Journal 97 (2000) 322–330. doi:10.14359/863.

[26] M. A. Ali, R. N. White, Structural Journal 98 (2001) 431–442. doi:10.14359/10286.

[27] M. Bruggi, Computers & Structures 87 (2009) 1483–1495. doi:10.1016/j.compstruc.2009.06.003.

[28] A. T. Gaynor, J. K. Guest, C. D. Moen, Journal of Structural Engineering 139 (2012) 607–618.

[29] M. Baandrup, O. Sigmund, H. Polk, N. Aage, Nature Communications 11 (2020) 1–7.

[30] M. P. Bendsøe, O. Sigmund, Archive of applied mechanics 69 (1999) 635–654.

[31] A. T. Gaynor, N. A. Meisel, C. B. Williams, J. K. Guest, Journal of Manufacturing Science and Engineering 136 (2014) 061015–1–061015–10.

[32] S. Watts, D. A. Tortorelli, International Journal for Numerical Methods in Engineering 108 (2016) 1498–1524.

[33] G. Cheng, Structural optimization 10 (1995) 173–179.

[34] G. I. Rozvany, Structural optimization 11 (1996) 213–217.

[35] M. Zhou, Structural optimization 11 (1996) 134–136.

[36] W. Achtziger, Structural optimization 17 (1999) 247–258.

[37] X. Guo, G. Cheng, K. Yamazaki, Structural and Multidisciplinary Optimization 22 (2001) 364–373.

[38] A. Ben-Tal, F. Jarre, M. Kočvara, A. Nemirovski, J. Zowe, Optimization and Engineering 1 (2000) 189–213.

[39] M. Kočvara, Structural and multidisciplinary optimization 23 (2002) 189–203.

[40] M. Jalalpour, T. Igusa, J. K. Guest, International Journal of Solids and Structures 48 (2011) 3011–3019.

[41] W. Achtziger, Structural optimization 12 (1996) 63–74.

[42] M. Stolpe, K. Svanberg, Structural and Multidisciplinary Optimization 27 (2004) 126–129.

[43] S. Rakshit, G. Ananthasuresh, Structural and Multidisciplinary Optimization 35 (2008) 55–68.

[44] W. Dorn, R. Gormory, H. Greenberg, J. de Mecanique 3 (1964) 25–52.

[45] MATLAB, version (2020b), The MathWorks Inc., Natick, Massachusetts, 2020.

[46] M. Ohsaki, Optimization of finite dimensional structures, CRC Press, 2011.

[47] M. Stolpe, Structural and Multidisciplinary Optimization 53 (2016) 349–374.

[48] I. Grossman, V. Voudouris, O. Ghattas, in: C. Floudas, P. Pardalos (Eds.), Recent Advances in Global Optimization, Princeton University Press, 1992.

[49] M. Stolpe, Optimization and Engineering 8 (2007) 163–192.

[50] K. Mela, Structural and Multidisciplinary Optimization 50 (2014) 1037–1049.

[51] R. Van Mellaert, G. Lombaert, M. Schevenels, Journal of Structural Engineering 142 (2016) 04015120.

[52] H. Fairclough, M. Gilbert, Structural and Multidisciplinary Optimization (2020) 1–23.

[53] M. Bruggi, Structural and multidisciplinary optimization 36 (2008) 125–141.

[54] B. Xia, J. Xiao, T. Ding, K. Zhang, Structural Safety 92 (2021) 102103.

[55] M. P. Bendsøe, Structural Optimization 1 (1989) 193–202.

[56] American Institute of Steel Construction, American Institute of Steel Construction (????).

[57] G. Sved, Z. Ginos, International Journal of Mechanical Sciences 10 (1968) 803–805.

[58] U. Kirsch, Structural optimization 2 (1990) 133–142.

[59] G. D. Cheng, X. Guo, Structural optimization 13 (1997) 258–266.

[60] G. Rozvany, Structural and Multidisciplinary Optimization 21 (2001) 164–172.

[61] W. Achtziger, C. Kanzow, Mathematical Programming 114 (2008) 69–99.

[62] J. S. Arora, Introduction to optimum design, 4 ed., Academic Press, 2017.

[63] B. Xu, A. Bouchaïr, M. Taazount, E. Vega, Engineering Structures 31 (2009) 2357–2367.

[64] A. Hassanieh, H. Valipour, M. Bradford, Construction and Building Materials 118 (2016) 63–75.

[65] W. S. Hemp, Optimum structures, Clarendon Press, 1973.

[66] J. E. Kelley, Jr, Journal of the society for Industrial and Applied Mathematics 8 (1960) 703–712.

[67] D. M. Frangopol, M. Soliman, Structure and infrastructure engineering 12 (2016) 1–20.

[68] B. Xia, T. Ding, J. Xiao, Waste Management 105 (2020) 268–278.

[69] J. Liu, Y. Ma, Journal of mechanical design 139 (2017) 011403.